Quasi-Steady Endless Vortices with Chaotic Streamlines

Oscar Velasco Fuentes

Abstract This chapter reviews the dynamics of one or more endless vortices in an incompressible inviscid fluid. Each vortex, a thin closed tube lying on the surface of an immaterial torus, is characterised by the number of turns, p, that it makes round the torus symmetry axis and the number of turns, q, that it makes round the torus centerline. Since the vortices are assumed to be identical and evenly distributed on any meridional section of the torus, the flow evolution depends only on the vortex topology (p, q), the number of vortices (n) and the torus thickness $(r_1/r_0$, where r_0 is the centerline radius and r_1 is the cross-section radius). Numerical simulations based on the Biot-Savart law showed that a small number of vortices ($n = 1, 2, 3$) coiled on a thin torus ($r_1/r_0 \leq 0.16$) progressed along and rotated around the torus symmetry axis in an almost uniform manner while each vortex approximately preserved its shape. In the comoving frame the velocity field always possesses two stagnation points. The stream tube emanating from the front stagnation point and the stream tube ending at the rear stagnation point intersect along a finite number of stream lines, giving rise to a three-dimensional chaotic tangle. It was found that a single toroidal vortex $\mathscr{V}_{p,q}$ generates a larger chaotic region if it makes less coils round the symmetry axis (smaller p) or if it lies on a thicker torus (larger r_1/r_0). Similarly a set of linked ring vortices $\mathscr{V}_{11}$ generate a larger chaotic region if there are less vortices in the set (smaller n) or if they lie on a thicker torus (larger r_1/r_0).

1 Introduction

An endless vortex is a mass of fluid rotating round a closed curve. The best known example is the *smoke ring*, which is a vortex whose axis of rotation is approximately circular. Ring vortices have been observed for over 400 years in man-made situations, like the firing of cannons or the puffing of tobacco smoke, and possibly longer

O. Velasco Fuentes (✉)
CICESE, Ensenada, México
e-mail: ovelasco@cicese.mx

J. Klapp and A. Medina (eds.), *Experimental and Computational Fluid Mechanics*, Environmental Science and Engineering, DOI: 10.1007/978-3-319-00116-6_8,

in natural situations, like the exhalations of volcanoes and geysers. The earliest references to smoke rings appeared at the dawn of the seventeenth century in the writings of English dramatists, and soon afterwards the first graphical representations of them appeared in the works of Dutch painters (Velasco Fuentes 2013). Despite this ancient interest, it was seemingly not until the beginning of the nineteenth Century that it was recognised that the mysterious smoke rings are in fact vortices. At this time it was even suggested that their motion is responsible for their stability and capacity to carry fluid (B 1804): the "quick rotation of the ring, from within outwards, (...) seems, in some manner or another, as if it kept the parts together." In the following decades the interest in smoke rings increased to such an extent that Helmholtz (1858) and Rogers (1858) published, with only a few months of difference, an analytical study of the motion of *kreisförmige Wirbelfäden* (circular vortex-filaments) and an experimental study of the formation of *rotating rings*, respectively.

A few years later Kelvin (1867a) placed the ring vortex in a prominent scientific position with his hypothesis that matter consists of *vortex atoms* moving in an all-pervading ideal fluid. This turned out to be an erroneous conjecture, but it also proved to be very fruitful for fluid mechanics and mathematics. Indeed, the major advances on vortex dynamics in the following decades were made in the pursuit of the vortex atom theory (e.g., the Kelvin circulation theorem, Kelvin waves on a cylindrical vortex, the stability of a polygon of point vortices, the motion of ring vortices, etc.). And the theory of knots, now one of the most active areas of research in mathematics, received a decisive impulse from the speculations of Kelvin and Peter Guthrie Tait about the shapes that these vortex atoms could take.

One of the first things Kelvin wondered about was the motion of linked ring vortices. On 22 January 1867 he wrote to Helmholtz that he was "a good deal puzzled as to what two vortex-rings through one another would do (how each would move, and how its shape would be influenced by the other)" (Thompson 1910). Kelvin (1875) later deduced that specific configurations of individual as well as multiple endless vortices could rotate and advance uniformly along a fixed line without changing their shape. Kelvin did not give the exact configuration of these steady vortices but hypothesized that they should be thin tubular vortices uniformly coiled on an immaterial torus so that each vortex winds p times around the torus' symmetry axis and q times around the torus' centerline before closing on itself (see Fig. 1).

Building on Kelvin's hypothesis, Thomson (1883) analysed the motion of two or more toroidal vortices. He obtained an approximate analytical expression for the shape and translation speed of two steady, linked vortices of equal circulation. And by considering the limit of infinitely thin vortices lying on the surface of a torus of infinite centerline radius, Thomson (1883) obtained his celebrated result about the stability of a regular polygon of n equal point-vortices.

Almost a century later, Kida (1981) found steady vortex solutions under the local-induction approximation (LIA, an approximation that amounts to omitting distant effects when computing the vortex' self-induced velocity, which then turns out to be proportional to the local curvature of the filament). In the LIA solutions of Kida (1981) the supporting torus may have an oval cross section but steady vortices exist only when $q \geq p$. Ricca et al. (1999) studied the evolution of these vortices under

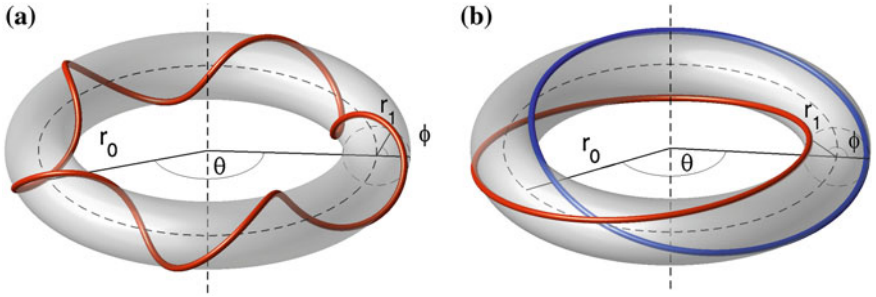

Fig. 1 Thin tubular vortices coiled on an immaterial torus represented by the *grey surface*. **a** A toroidal helix coiled once round the torus symmetry axis and five times round the torus centerline. **b** Two linked ring vortices, each one coiled once round the torus symmetry axis and once around the torus centerline. Right frame adapted from Velasco Fuentes and Romero Arteaga (2011)

both the Biot-Savart law and the LIA: the numerical simulations based on the Biot-Savart law confirmed the hypothesis of Kelvin (1875) whereas those based on LIA were consistent with the analytical results of Kida (1981).

Recently Kleckner and Irvine (2013) succeeded in generating, in a controlled and systematic way, knotted, unknotted and linked vortices in water. Their toroidal helical vortices were stable, the more complicated vortices rapidly became unstable and underwent topological changes through reconnection. The probable cause of these results is that neither the couple of ring vortices nor the trefoil-knot vortex were, in their initial condition, close to the steady solutions hypothesised by Kelvin.

Here we review published results on the dynamics of knotted and unknotted vortices (Velasco Fuentes 2010) and of linked vortices (Velasco Fuentes and Romero Arteaga 2011). Two aspects are central in this review: the vortices' steadiness, that is to say the uniformity of their motion and the constancy of their shapes; and the vortices' capacity to carry fluid, that is to say, the existence of three-dimensional islands of stability surrounding the vortices. In Sect. 2 we discuss the conservation laws discovered by Kelvin, which were the basis for his deductions. The numerical results of Sect. 3 confirm that thin tubular vortices coiled on a torus according to Kelvin's prescriptions are quasi-steady. In Sect. 4 we analyse the velocity field and the transport properties of toroidal vortices. Section 5 contains some conclusions.

2 Integrals of Motion

We assume that the vortices evolve in an inviscid, incompressible, homogeneous fluid which is unbounded and acted upon by conservative forces only. Therefore the kinetic energy, E, and the linear an angular vortex impulses, $\mathbf{I}$ and $\mathbf{A}$ respectively, are invariants of the motion. If all vorticity is concentrated on a single line vortex, these conserved quantities are defined as follows:

$$E = \frac{1}{2}\Gamma \oint \mathbf{u} \cdot \mathbf{R} \times d\mathbf{s} \tag{1}$$

$$\mathbf{I} = \frac{1}{2}\Gamma \oint \mathbf{R} \times d\mathbf{s} = \Gamma \int d\mathbf{S} \tag{2}$$

$$\mathbf{A} = -\frac{1}{2}\Gamma \oint R^2 d\mathbf{s} = \Gamma \int \mathbf{r} \times d\mathbf{S} \tag{3}$$

Here we have used standard notation: the vortex has circulation Γ, moves with velocity $\mathbf{u}$, and lies on the three-dimensional curve $\mathbf{R}(s)$; $d\mathbf{s}$ is a line element along this curve and $d\mathbf{S}$ is the surface element at the point $\mathbf{r}$ of an arbitrary surface spanning the closed curve $\mathbf{R}(s)$.

Kelvin (1869) demonstrated the conservation of linear and angular vortex impulses in the general case, and discovered their geometric meaning when the vorticity is concentrated on a set of filamentary vortices (Kelvin 1875). To achieve this, he first introduced the following definitions:

1. The resultant area of a 3D closed curve is the area of its projection on the plane that makes this projection a maximum.
2. The resultant axis of this curve is the line that passes through its centre of gravity and is perpendicular to the plane of its resultant area.
3. The areal moment of a 2D surface about any axis is equal to its area multiplied by the distance between that axis and the line passing perpendicularly through the surface's centroid.
4. The resultant areal moment of a 3D closed curve is equal to the moment, about the curve's resultant axis, of the areas of its projections on two mutually orthogonal planes that are parallel to this axis.

With these definitions Kelvin (1875) was able to spell out Eqs. (2)–(3) in the form of two theorems:

Theorem 1 *The linear impulse of a curvilinear vortex of unit circulation is equal to its resultant area.*

Theorem 2 *The angular impulse of a curvilinear vortex of unit circulation is equal to its resultant areal moment.*

These theorems, combined with the conservation of linear and angular impulses, allowed Kelvin (1875) to give the following description of the behaviour of a filamentary vortex of arbitrary shape: "the resultant area, and the resultant areal moment of the curve formed by the filament, remain constant however its curve may become contorted; and its resultant axis remains the same line in space. Hence, whatever motions and contortions the vortex filament may experience, if it has any motion of translation through space this motion must be in average along the resultant axis."

Antecedents of these results can be traced back to Helmholtz and Maxwell. The former showed that in a purely azimuthal vorticity field the sum of the projected areas of all ring elements, multiplied by their vorticity, is constant (Helmholtz 1858). The latter, writing to Tait in July 1868, stated that "two ring vortices of any form affect each others area so that the sum of the projection of the two areas on any plane remains constant" (Maxwell and Harman 1995).

2.1 Numerical Method

We compute the vortex motion with the Rosenhead-Moore approximation to the Biot-Savart law (Saffman 1995):

$$\mathbf{u}(\mathbf{x}) = -\frac{\Gamma}{4\pi}\sum_i \oint \frac{[\mathbf{x}-\mathbf{R}_i(s)]\times d\mathbf{s}}{\left(|\mathbf{x}-\mathbf{R}_i(s)|^2+\mu^2 a^2\right)^{3/2}}, \tag{4}$$

The use of this approximation implies that the vortices are no longer infinitely thin: they now have an undeformable, circular cross-section of radius a. The value of the radius is chosen to be $a = 0.05 r_0$, that of the constant μ depends on the vortex internal structure. The particular value used here, $\mu = e^{-3/4}$, corresponds to uniform vorticity on the vortex cross section (Saffman 1995).

In order to evaluate the integral on the right-hand side, we represented each vortex with a set of material markers. We chose the number of markers as $m \approx 2L/a$, where L is the vortex length, and the time step as $dt \approx a^2/\Gamma$, because preliminary tests showed that these values resulted in accurate simulations of the motion of a circular ring, i.e. the shape was preserved and the speed deviated less than 0.5 % from the analytical value. Higher spatial or temporal resolutions substantially increased the computational costs without providing major improvements in the accuracy. Since the vortices evolved without significant changes in length or shape it was not necessary to update the spatial discretization as is usually done in highly time-dependent flows (see, e.g., Baggaley and Barenghi 2011).

We used a fourth-order Runge-Kutta scheme with fixed time step to integrate the evolution equation

$$\frac{d\mathbf{x}_k}{dt} = \mathbf{u}(\mathbf{x}_k, t),$$

where $\mathbf{x}_k$ is the position of the node and $\mathbf{u}(\mathbf{x}_k, t)$ is its velocity, computed with equation (4). Note that k runs through all nodes ($j = 1, \ldots, m$) of all filaments ($i = 1, \ldots, n$). To verify the accuracy of the simulations, we monitored the evolution of the integrals of motion (1)–(3): the energy varied by less than 0.1 % of its initial value; the linear and angular impulses varied by less than 0.001 and 0.1 % of their initial magnitudes, respectively, while their directions, which initially coincided with the torus symmetry axis, deviated from this direction by angles of about 0.0001 s.

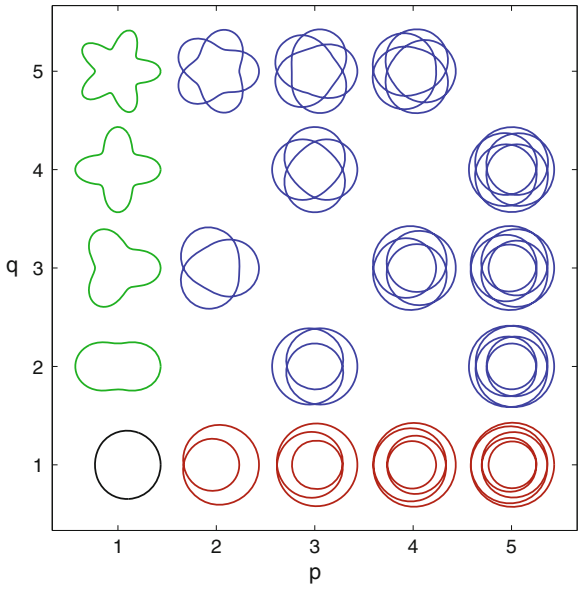

Fig. 2 Topology of toroidal vortices as a function of p and q: ring (*black*), helices (*green*), loops (*red*), and knots (*blue*)

2.2 Initial Conditions and Parameter Space

Following Kelvin (1875) we assume that a number of identical tubular vortices of small cross-section are uniformly coiled on a torus whose centerline has a radius r_0 and whose cross-section has a radius r_1. In Cartesian coordinates the centerline of the vortex is given as follows:

$$\begin{aligned} x &= (r_0 + r_1 \cos\phi)\cos\theta, \\ y &= (r_0 + r_1 \cos\phi)\sin\theta, \\ z &= r_1 \sin\phi. \end{aligned}$$

where ϕ is the angle round the torus centerline and θ is the angle round the torus symmetry axis (see Fig. 1). They are given by $\phi = qs - 2(n-i)\pi/n$ and $\theta = ps$, where n is the number of vortices, i indicates the vortex being described, p and q are co-prime integers and s is a parameter in the range $0 - 2\pi$. Therefore, before closing on itself, each vortex $\mathscr{V}_{p,q}$ makes p turns round the torus symmetry axis and q turns round the torus centerline. These numbers determine the topology of the vortex, as follows: when $p > 1$ and $q > 1$ the vortex forms a toroidal knot, when either $p = 1$ or $q = 1$ the vortex forms a toroidal unknot (see Fig. 2). In the latter situation it is useful to make a further distinction between toroidal helices ($p = 1$ and $q > 1$), and toroidal loops ($p > 1$ and $q = 1$).

When there are two or more vortices in a given configuration, all of them have the same circulation, Γ, and topology, p, q. Equal circulations are necessary for

the steadiness of motion; equal topologies are necessary to avoid an intersection of the vortices, which would be in violation of the condition $\nabla \cdot \omega = 0$. Note also that the term $2(n-i)\pi/n$ ensures that the vortices are equally spaced on the section of the torus (i.e., they intersect any meridional plane on the vertices of a regular polygon inscribed on the corresponding cross-section of the torus).

Here we discuss the dynamics of a small number ($n < 5$) of toroidal vortices ($\mathscr{V}_{pq}$) coiled on thin tori ($r_1/r_0 < 0.16$). We must further set a lower bound for r_1/r_0 because of the desingularization of the Biot-Savart law, which implies that the vortices have an undeformable cross-section of radius a. Consistency then requires that the vortices are never too close to each other, i.e. their centerlines must be separated by distances about or larger than $3a$. We chose to use a value which amply satisfies this condition for $n = 2$ and narrowly does it for $n = 4$. Therefore in this study the aspect ratio of the torus will be in the range $0.1 < r_1/r_0 < 0.16$ (except for one case in Sect. 4).

3 Vortex Motion

3.1 Knotted and Unknotted Vortices

Figure 3 shows the evolution of a trefoil-knot vortex ($\mathscr{V}_{23}$). The vortex, initially coiled on a thin torus ($r_1/r_0 = 0.1$), progresses along the torus' symmetry axis (the thin line in the lateral view) while rotating around the same axis (the cross in the front view). As predicted by Kelvin (1875), all vortices $\mathscr{V}_{pq}$ coiled on thin tori are observed to progress and rotate in an approximately uniform manner. The linear speed, U, is proportional to p and is almost unaffected by the value of q (Fig. 4, left panel). This behaviour is easily explained as follows: since $r_1/r_0 = 0.1$ the progression speed behaves as if there was a single ring with circulation $p\Gamma$ instead of p loops of a filament with circulation Γ. As a matter of fact $U \approx 3/4\, pU_0$, where U_0 is the speed of a circular ring of strength Γ and radius r_0 (Kelvin 1867b):

$$U_0 = \frac{\Gamma}{4\pi r_0}\left[\log\frac{8r_0}{a} - \frac{1}{4}\right] \tag{5}$$

The angular speed, Ω, grows with increasing p and decreasing q (Fig. 4, right panel). Note that toroidal helices ($p = 1$) rotate in the opposite sense and at a much lower rate than toroidal loops ($q = 1$); and toroidal knots rotate in the same sense and at lower rates than toroidal loops.

3.2 Linked Vortices

Figure 5 shows the evolution of a pair of linked ring vortices $\mathscr{V}_{11}$ of equal circulation. The vortices were initially coiled on a thin torus ($r_1/r_0 = 0.1$). The lateral

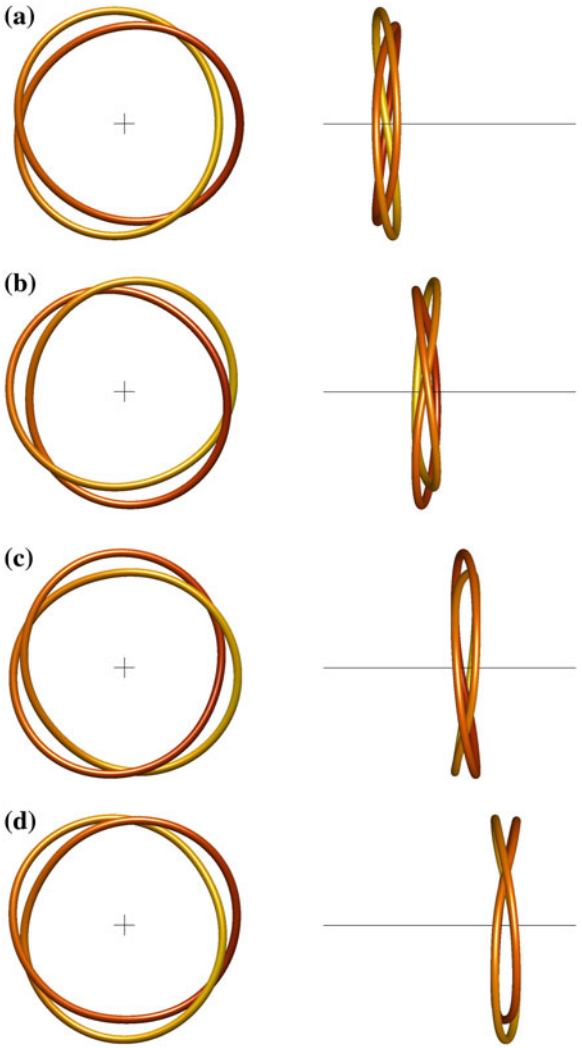

Fig. 3 Evolution of a trefoil-knot vortex $\mathscr{V}_{23}$ with $r_1/r_0 = 0.1$. The axis of the system is represented by a cross in the frontal view (*left-hand side column*) and by a straight line in the lateral view (right-hand side column). The stages depicted are (**a**) $t = 0$, (**b**) $t = 0.23T$, (**c**) $t = 0.46T$, (**d**) $t = 0.69T$, where T is the time required by a circular ring vortex of centerline radius r_0 and cross-section radius a to advance a distance equal to r_0

view shows the progression of the vortices along the torus' symmetry axis whereas the front view shows the rotation of the vortices around the same axis. This figure shows exactly one vortex rotation and since this is relatively fast, the vortices are seen to advance only a short distance during this time. They, however, continue rotating and progressing in the same way for much longer times. Figure 6, for example, shows the vortices advancing a distance equal to eight-times their diameter while

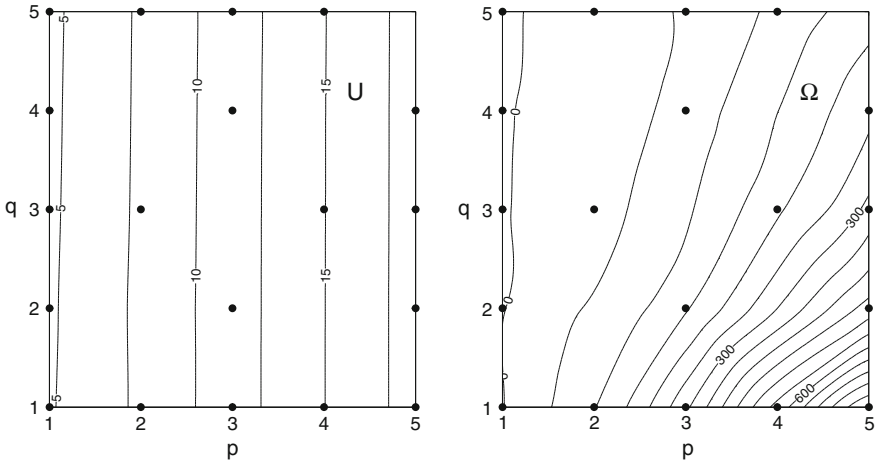

Fig. 4 Linear speed (U) and angular speed (Ω) of the vortex system as functions of p and q. The speed of linear motion along the torus axis, U, is scaled by $\Gamma/4\pi r_0$; the angular speed of rotation round the torus axis, Ω, is scaled by $\Gamma/2\pi r_0 r_1$. The *black dots* indicate the only points where toroidal vortices exist. The contours of U and Ω were drawn by interpolation to show how these speeds change in the parameter space. Taken from Velasco Fuentes (2010)

performing almost sixteen rotations around their symmetry axis. The bottom row of the same figure shows the corresponding time evolution of quantities that, theoretically, should be conserved but which are not exactly so in the numerical simulations. Instead of the instantaneous values of the energy and the linear and angular impulses, Eqs. (1)–(3), we plotted their relative change; thus Fig. 6 shows, respectively, $E(t)/E(0) - 1$, $|\mathbf{I}(t)|/|\mathbf{I}(0)| - 1$ and $|\mathbf{A}(t)|/|\mathbf{A}(0)| - 1$. In the period shown, the energy is preserved within 0.01 %, the linear impulse within 0.001 %, and the angular impulse within 0.02 %.

The progression of the vortices corresponds, because of Helmholtz (1858) vortex laws, with the advance of material elements. The vortex rotation around the symmetry axis does not match a similar motion of material elements: it is actually an azimuthal wave. To verify this, note that the hue of the colour marks fluid elements along each vortex and that, in the front view, the darker hues remain on the right-hand side and the lighter ones on the left-hand side of the vortices. The cause of the azimuthal wave is a different motion of the material elements, namely their rotation around the torus centerline. This can be qualitatively verified by close inspection of the vortices' lateral view in Fig. 6.

Hence the motion of the fluid elements that make up the vortices has two main components: (a) progression along the torus' symmetry axis, and (b) rotation around the torus' centerline. We found that these components are approximately uniform so that we characterised them by the average speeds U and Ω_c, respectively.

The linear speed U grows with the number of vortices n and decreases with the aspect ratio r_1/r_0. A simple argument accounts for this: since $r_1/r_0 << 1$ the

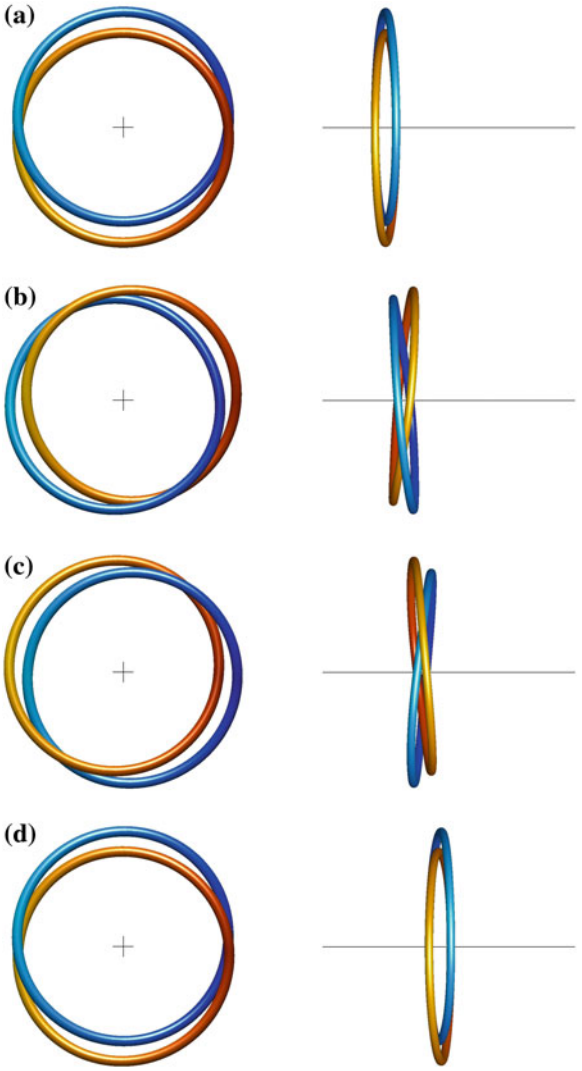

Fig. 5 Evolution of two linked ring vortices $\mathscr{V}_{11}$ with $r_1/r_0 = 0.1$. The axis of the system is represented by a cross in the frontal view (*left-hand side column*) and by a straight line in the lateral view (*right-hand side column*). The stages depicted are (**a**) $t = 0$, (**b**) $t = 0.105T$, (**c**) $t = 0.210T$, (**d**) $t = 0.315T$, where T is the time required by a circular ring vortex of centerline radius r_0 and cross-section radius a to advance a distance equal to r_0. Taken from Velasco Fuentes and Romero Arteaga (2011)

progression speed behaves as if, instead of n toroidal rings with circulation Γ, there was a single circular ring with cross-section radius r_1 and circulation $n\Gamma$. The speed of this virtual vortex is $U_0 = (n\Gamma/4\pi r_0)[\log(8r_0/r_1) - 1/4]$. Figure 7 shows that

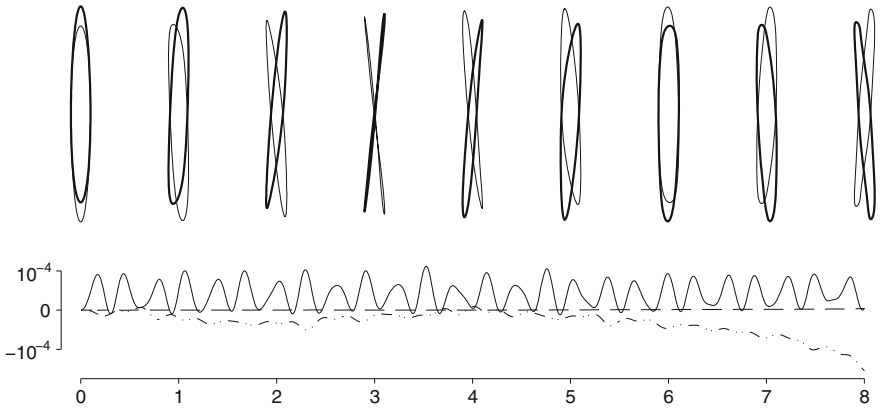

Fig. 6 *Top* Progressive motion of a pair of linked vortices (the same of Fig. 5 but for a 16-times longer period). *Bottom* Time evolution of the kinetic energy E (*continuous line*), linear impulse $\mathbf{I}$ (*dashed line*), and angular impulse $\mathbf{A}$ (*dot-dashed line*). The relative change of these quantities (see text) is shown as a function of the adimensional distance travelled by the vortices, $Z = Ut/r_0$ (where U is the speed of the vortices, t is the time and r_0 is the torus' centerline radius). Taken from Velasco Fuentes and Romero Arteaga (2011)

this is in good agreement with the speeds measured for sets of linked ring vortices, particularly when $n = 2$.

The angular speed Ω_c increases with n and decreases with r_1/r_0. This can be explained following (Thomson 1883): since the vortices are thin and $r_1/r_0 << 1$ they move on the meridional plane as if they were a set of point vortices. Indeed, in the parameter region studied here, $\Omega_c \approx 0.94\Omega_0$, where Ω_0 is the angular speed of a set of n point vortices of circulation Γ placed on the vertices of a regular polygon inscribed on a circle of radius r_1: $\Omega_0 = (n-1)\Gamma/4\pi {r_1}^2$. We argued above that the material rotation around the torus' centerline causes the azimuthal wave around the torus' symmetry axis. The close agreement, shown in Fig. 7, between Ω_0 and the angular speed of the azimuthal wave, Ω, quantitatively demonstrates the connection between these two rotations.

We applied several diagnostics to measure the deformation of the vortices throughout their evolution. The simplest one was the time evolution of the vortex length, which was observed to vary within 0.3 % of its initial value in the region of the parameter space studied here ($n = 2, 3$ and $0.1 \leq r_1/r_0 \leq 0.16$). The second diagnostic consisted in finding the torus that best fitted the vortices at every stage of the evolution. The conservation laws (2)–(3) guarantee that the fitting torus has the same symmetry axis as the initial one, therefore the former is uniquely determined by the radii $r_0(t)$ and $r_1(t)$. We found that $r_0(t)$ remained within 1 % of its initial value, whereas $r_1(t)$ remained within 5 % of its initial value. The final diagnostic was to measure the signed distance, Δr_1, from the surface of the torus to every material marker representing the vortices. The time series of histograms of Δr_1 showed that the markers remained within a distance $0.01r_0$ of the torus (as in the case $n = 2$, $r_1/r_0 = 0.1$, shown in Fig. 8).

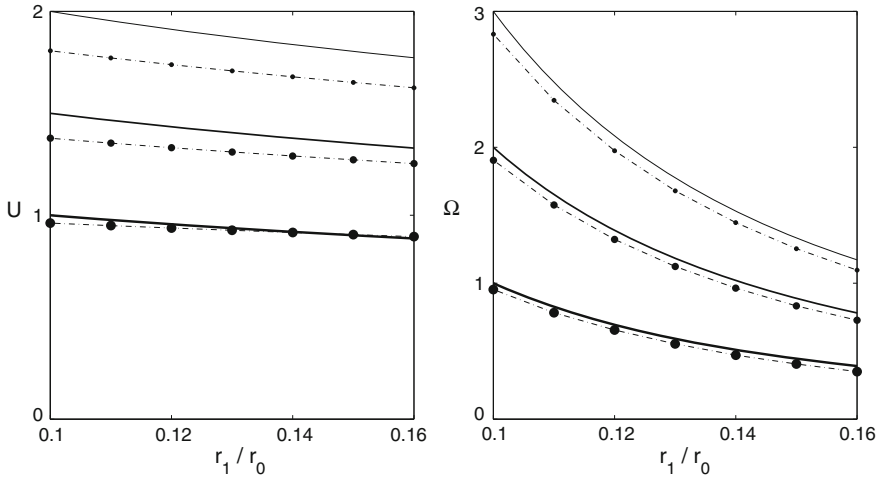

Fig. 7 Linear speed (U) and phase angular speed (Ω) of n linked vortices as functions of the torus aspect ratio (r_1/r_0), for sets of $n = 2$ (*thickest line and largest markers*), $n = 3$ and $n = 4$ (*thinnest line and smallest markers*). The continuous lines represent the analytical functions discussed in the text, the markers represent the results of the numerical simulations. The linear speeds are scaled by the speed of a circular ring vortex of circulation 2Γ, centerline radius r_0 and cross section radius $2a$, the angular speeds are scaled by the rotation speed of a pair of point vortices of circulation Γ separated by a distance $4a$. Taken from Velasco Fuentes and Romero Arteaga (2011)

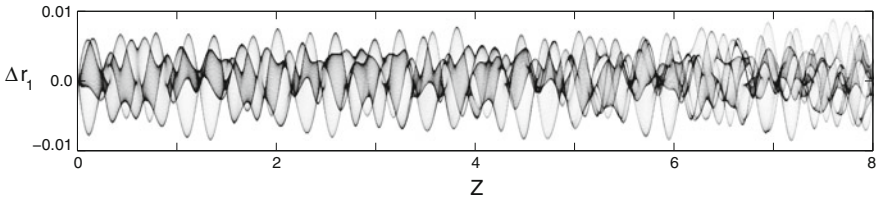

Fig. 8 Evolution of the vortex shape as illustrated by a time series of the histogram of distances from the vortex markers to the surface of the torus (see text). The signed distance, Δr_1, at which a certain percentage of the markers is located (*white*: 0 %; *black*:100 %) is shown as a function of the adimensional distance travelled by the vortices, $Z = Ut/r_0$ (where U is the speed of the vortices, t is the time and r_0 is the torus' centerline radius). The results correspond to the simulation shown in Fig. 6. Taken from Velasco Fuentes and Romero Arteaga (2011)

4 Flow geometry

The toroidal vortices discussed in the previous section very nearly keep their shape and are almost stationary when observed in a frame that translates with speed U and rotates with angular speed Ω. Hence we will use this comoving frame to analyse the geometry of the velocity field. Since the vortices lie on a thin torus the velocity field they produce may be regarded as a small perturbation of the velocity field of a circular ring vortex, at least away from the immediate vicinity of the vortices.

Hence we describe first the flow geometry of a circular ring vortex of radius r_0 and cross section r_1 in the comoving system (i.e. progressing with speed U). The flow may qualitatively change depending on the numerical value of r_1/r_0 but all values used here fall within the regime of *fat* ring vortices ($r_1/r_0 > 1/86$, see Saffman 1995 for a detailed analysis). In this regime the velocity field has two stagnation points, both lying on the ring's symmetry axis. The forward one, P, has a linear attractor and a planar repellor; the backward one, Q, has a linear repellor and a planar attractor. The two stagnation points are connected by an infinite number of streamlines starting at P and ending at Q. These lines form a surface with the shape of an oblate spheroid. This stream surface is called separatrix, because the streamlines located inside it are qualitatively different from those located outside it: the former are closed whereas the latter are open and of infinite length. From a more physical point of view, the separatrix is the surface that divides the ambient fluid from the fluid permanently carried by the vortex.

The addition of a solid body rotation, Ω, round the symmetry axis affects neither the existence nor the position of the stagnation points. The rotation transforms the plane streamlines into helical curves but it leaves the shapes of all stream surfaces unaltered. Therefore, the separatrix of a circular ring vortex in a system progressing with speed U and rotating with speed Ω is the same oblate spheroid described above.

Let us now see what happens when we substitute back the toroidal vortices in the place of the virtual ring vortex. The stagnation points survive, although somewhat displaced. The separatrix, in contrast, disappears: instead of a single surface starting at P and ending at Q, there are now two surfaces. The first one, called the unstable manifold, starts at P and ends infinitely far downstream; the second one, called the stable manifold, starts infinitely far upstream and ends at Q. These surfaces intersect along a finite number of streamlines which start at P and end at Q.

We obtained the unstable manifold by computing a set of streamlines starting on the vicinity of the front stagnation point. The starting points lay on a circle of small radius ($0.01r_0$), coaxial with the torus and centred at the stagnation point. The stable manifold could have been computed in a similar way, but this was unnecessary. Note that a time reversal in the equations of motion is equivalent to a change of sign of all vortex circulations (i.e. $\Gamma \rightarrow -\Gamma$) and this is equivalent to the transformation $(x, y, z) \rightarrow (x, -y, -z)$, because of the initial conditions described in Sect. 2.2. Therefore, to obtain the stable manifold, we rotated the unstable one by an angle π around the x axis.

In the vicinity of the vortices the flow is always very different from that of a ring vortex. In order to study the geometry of the flow in this region, we used Poincaré sections. We constructed these by numerically computing a set of streamlines that started on a radial line going from the vicinity of the torus symmetry axis to the vicinity of the vortices, and plotting every intersection of the streamlines with the meridional plane that contains the starting points.

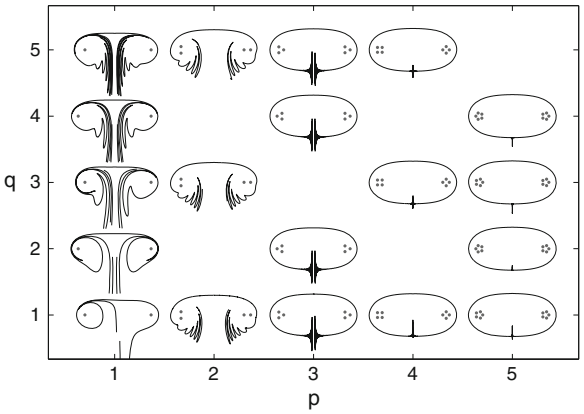

Fig. 9 The unstable manifold of toroidal vortices $\mathscr{V}_{p,q}$. All vortices have small cross-section ($a/r_0 = 0.05$) and are coiled on a thin torus ($r_1/r_0 = 0.1$); their intersections with the meridional planes $\theta = 0, \pi$ are represented by *grey dots*. Taken from Velasco Fuentes (2010)

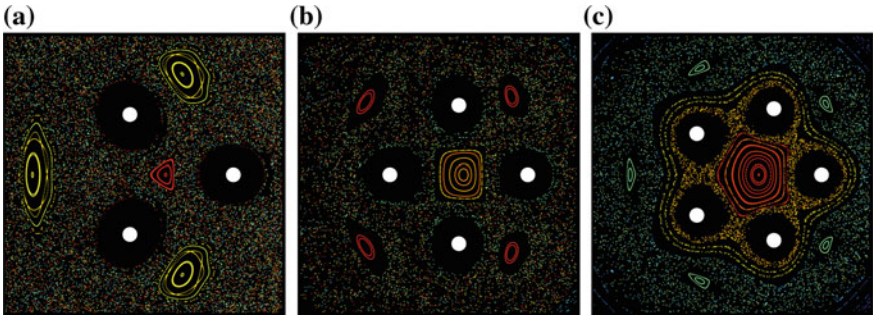

Fig. 10 Poincaré sections of streamlines induced by toroidal vortices: (**a**) $\mathscr{V}_{3,1}$, (**b**) $\mathscr{V}_{4,1}$ and (**c**) $\mathscr{V}_{5,1}$. The intersections of the vortices with the meridional plane $\theta = 0$ are represented by white circles, those of the streamlines by dots coloured according to the position of the streamline's starting point (*blue*: closer to the torus' symmetry axis; *red*: closer to torus centerline). Adapted from Velasco Fuentes (2010)

4.1 Knotted and Unknotted Vortices

Figure 9 shows meridional cross-sections of the unstable manifold for all toroidal vortices in the range $1 < p < 5$ and $1 < q < 5$. The shape of the manifolds is mainly determined by p, whereas the value of q is important only for toroidal helices ($p = 1$). Note, for example, that the manifold of the knotted vortex $\mathscr{V}_{2,5}$ is more similar to that of the unknotted vortex $\mathscr{V}_{2,1}$ than to the knotted vortex $\mathscr{V}_{3,5}$. As p grows the oscillations of the unstable manifold start closer to the backward stagnation point Q. When $p > 3$ the unstable and stable manifolds differ very little (except in the immediate neighbourhood of P and Q) from the separatrix of a fat ring vortex.

The Poincaré sections show at least $2p$ large islands of stability: p correspond to the single tube of fluid permanently trapped by the vortex, and p correspond to a single tube of irrotational fluid which runs parallel to the vortex and has approximately the same shape (see Fig. 10). When $p > 2$ there is an additional island of stability which corresponds to a tube of irrotational fluid that surrounds the torus centerline. When $p = 1, 2$ all these tubes are embedded in the unbounded chaotic sea generated by the intersections of the manifolds. When $p > 2$ the tubes are embedded in a chaotic sea that is itself bounded by a KAM-like torus.

4.2 Linked Vortices

Figure 11 shows meridional cross sections of the stable and unstable manifolds of two linked vortices; each frame corresponds to a supporting torus of a particular aspect ratio ($r_1/r_0 = 0.07, 0.1$). In both cases the red curve, which represents the unstable manifold of P, smoothly moves downstream but, as it approaches Q, it starts to oscillate about the blue curve, which represents the stable manifold of Q. Similarly, the stable manifold of Q smoothly moves upstream but as it approaches P it starts to oscillate about the unstable manifold of P. Note that when the supporting torus is thinner (frame a, $r_1/r_0 = 0.07$) the oscillations of the manifolds are of small amplitude and they start close to the opposite stagnation point. In contrast, when the supporting torus is thicker (frame b, $r_1/r_0 = 0.10$) the oscillations of the manifolds are of larger amplitude and they start closer to their own stagnation point.

The presence of this geometric structure, known as heteroclinic tangle, implies that streamlines are chaotic in this region (Wiggins 1992). It also provides a template for the wandering of streamlines around different flow regions through the following mechanism (*lobe dynamics*, for details see Rom-Kedar et al. 1990). Consider two adjacent intersections, on some meridional plane, between the unstable manifold of P and the stable manifold of Q; the two line segments bounded by these points form a closed contour which defines an area, say A_1, usually called lobe (see Fig. 11b). The streamlines passing through A_1 successively intersect the same meridional plane within the lobes $A_2, A_3, \ldots$, thus reaching at some point the interior of the so-called vortex atmosphere. This is, however, only a transient situation because the same mechanism eventually brings them out to the downstream side of the vortex.

Figure 11b shows that there are two independent sequences of lobes, the green ones and the white ones, which implies that the unstable manifold of P intersects the stable manifold of Q along four streamlines. In fact we found that manifolds always intersect along $2n$ streamlines, where n is the number of vortices. Note also that here, as in all cases we have analysed, the areas of the lobes are larger when they are closer to the torus symmetry axis. This occurs because the fluid is incompressible and the azimuthal velocity grows with the distance to the torus axis.

Analogously to the case of a single vortex $\mathscr{V}_{pq}$, the Poincaré sections show at least $2n$ large islands of stability: n correspond to the tubes of fluid permanently trapped by an individual vortex, and n correspond to tubes of irrotational fluid which run parallel to the vortices and have approximately the same shape. When $n > 2$ there is

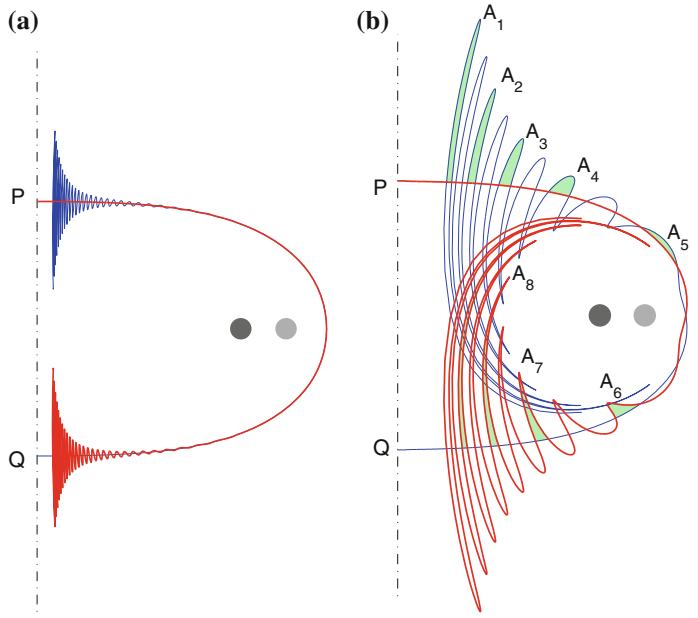

Fig. 11 Meridional cross section of the three-dimensional chaotic tangle of two linked ring vortices coiled on tori of different thickness: (**a**) $r_1/r_0 = 0.07$, (**b**) $r_1/r_0 = 0.10$. The *red* and *blue lines* represent, respectively, the unstable manifold of the front stagnation point (P), and the stable manifold of the rear stagnation point (Q); the *grey circles* represent the vortices and the *green* areas, labelled with A_i, represent successive intersections of a particular streamtube with the meridional plane (see text). Adapted from Velasco Fuentes and Romero Arteaga (2011)

an additional island of stability which corresponds to a tube of irrotational fluid that runs between the n vortices and surrounds the torus centerline.

If the number of vortices is large or the aspect ratio of the torus is small these islands of stability are embedded in a chaotic sea bounded by a nested set of KAM tori, as evidenced by the bands of differently coloured dots in Fig. 12a, c. Note that the largest KAM torus almost fills the "unperturbed" oblate spheroid. If, however, the number of vortices is small or the aspect ratio of the torus is large these islands of stability are embedded in an unbounded chaotic sea, as evidenced by the well mixed coloured dots in Fig. 12b, d.

5 Conclusions

Our numerical results confirm Kelvin (1875) deductions about knotted and linked toroidal vortices: they progress along and rotate around the torus symmetry axis with almost uniform speeds while undergoing negligible deformations. Although these results make plausible the existence of exact solutions which are both steady and stable, finding the analytical expression of such solutions is still an open problem.

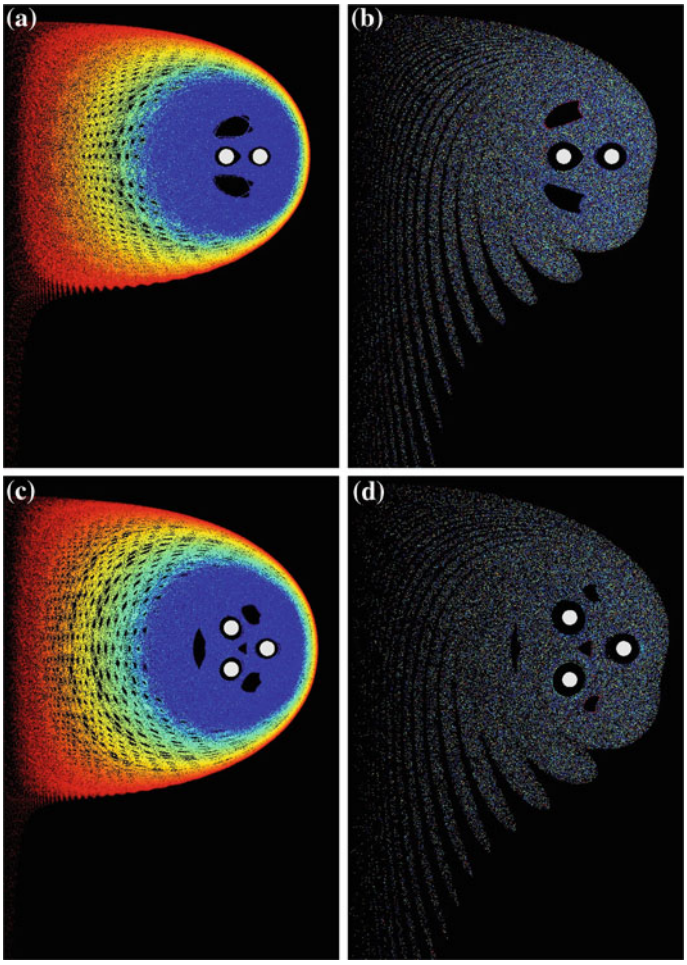

Fig. 12 Poincaré sections of streamlines in the velocity field of n linked ring vortices lying on tori of different thick nesses: **a** $n = 2$ and $r_1/r_0 = 0.07$, **b** $n = 2$ and $r_1/r_0 = 0.10$, **c** $n = 3$ and $r_1/r_0 = 0.10$, **d** $n = 3$ and $r_1/r_0 = 0.15$. The intersections of the vortices with the meridional plane $\theta = 0$ are represented by *white circles*, those of the streamlines by dots coloured according to the position of the streamline's starting point (*red*: closer to the torus' symmetry axis; *blue*: closer to the vortices). Taken from Velasco Fuentes and Romero Arteaga (2011)

The quasi-steadiness of the linked ring vortices enables us to interpret the results about the flow geometry in terms of the capacity of the vortices to carry fluid. We may thus conclude that a single toroidal vortex $\mathscr{V}_{p,q}$ carries more fluid if it makes more coils round the symmetry axis (larger p) or if it lies on a thinner torus (smaller r_1/r_0). Similarly a set linked ring vortices $\mathscr{V}_{11}$ carries more fluid if there are more vortices in the set (larger n) or if it lies on a thinner torus (smaller r_1/r_0).

Equation (4) shows that the velocity field depends on the value of μa, particularly in the neighbourhood of the vortices. This affects the self-induced velocity and,

through it, the flow geometry. For if μa is smaller the vortices move faster and their stagnation points are closer to each other, and vice versa. To evaluate the extent of the modifications produced by changing the value of μa, we used thinner vortices ($a = 0.025 r_0$) with the same internal structure used above ($\mu = e^{-3/4}$) and hollow vortices ($\mu = e^{-1/2}$) with the same cross-section used above ($a = 0.05 r_0$). The thinner vortices moved with a 6 %-larger speed and the distance between their stagnation points was 8 % smaller. The hollow vortices moved with a 3 %-smaller speed and the distance between their stagnation points was 4 % larger. In neither case the chaotic tangles or the Poincaré sections exhibited significant changes with respect to those shown in the present chapter.

References

B R (1804) On phosphoric rings. J Nat Philos, Chem Arts 7:64
Baggaley AW, Barenghi CF (2011) Spectrum of turbulent Kelvin-waves cascade in superfluid helium. Phys Rev B 83:134509
Helmholtz H (1858) Über Integrale der hydrodynamischen Gleichungen, welche den Wirbelbewegungen entsprechen. Journal für die reine und angewandte Mathematik 55:25–55
Helmholtz H (1867) On integrals of the hydrodynamical equations, which express vortex-motion. Phil Mag 33:485–512
Kida S (1981) A vortex filament moving without change of form. J Fluid Mech 112:397–409
Kleckner D, Irvine WTM (2013) Creation and dynamics of knotted vortices. Nat Phys doi:10.1038/nphys2560
Maxwell JC, Harman PM (1995) The scientific letters and papers of James Clerk Maxwell, vol 2. Cambridge University Press, Cambridge, pp 1862–1873
Ricca R, Samuels D, Barenghi C (1999) Evolution of vortex knots. J Fluid Mech 391:29–44
Rogers WB (1858) On the formation of rotating rings by air and liquids under certain conditions of discharge. Am J Sci Arts 26:246–258
Rom-Kedar V, Leonard A, Wiggins S (1990) An analytical study of transport, mixing and chaos in an unsteady vortical flow. J Fluid Mech 214:347–394
Saffman P (1995) Vortex dynamics. Cambridge University Press, Cambridge
Thompson SP (1910) The life of William Thomson Baron Kelvin of Largs. McMillan, London
Thomson JJ (1883) A treatise on the motion of vortex rings. MacMillan, London
Thomson W (Lord Kelvin) (1867a) On vortex atoms. Philos Mag 34:15–24. Also in mathematical and physical papers (MPP) 4:1–12
Thomson W (Lord Kelvin) (1867b) The translatory velocity of a circular vortex ring. Philos Mag 33:511–512. Also in MPP, 4:67–68
Thomson W (Lord Kelvin) (1869) On vortex motion. Trans R Soc Edinb 25:217–260. Also in MPP, 4:13–66
Thomson W (Lord Kelvin) (1875) Vortex statics. Proc R Soc Edinburgh 9:59–73. Also in MPP, 4:115–128
Velasco Fuentes O (2010) Chaotic streamlines in the flow of knotted and unknotted vortices. Theor Comput Fluid Dyn 24:189–193
Velasco Fuentes O (2013) Early observations and experiments on ring vortices. Eur J Mech B-Fluid. http://dx.doi.org/10.1016/j.euromechflu.2013.08.008
Velasco Fuentes O, Romero Arteaga A (2011) Quasi-steady linked vortices with chaotic streamlines. J Fluid Mech 687:571–583
Wiggins S (1992) Chaotic transport in dynamical systems. Springer-Verlag, Berlin